An Electromagnetic Field Model of Cardiac Excitation on Transverse Electric Current to Induce The Magnetic Field

Sehun Chun, *Member, IAENG,*

***Abstract*—Understanding the magnetic field distribution in the heart is crucial for interpreting electrocardiography (ECG) and magnetocardiography (MCG) results. However, its mathematical model has been restricted by the cardiac fibre orientation and has not been successful in some cases. In this paper, a novel electromagnetic model of cardiac electric signal propagation is proposed to provide a complete description of the magnetic field in multidimensional cardiac tissue which can be generated regardless of the cardiac fiber orientation. The derived Maxwell's equations, which are equivalent to those of the generic two-variable model, are identical to the classical electromagnetic field equations, but for a different medium, and provide a unified macroscopic propagation description of cardiac electric signal in multidimensional anisotropic space.**

***Index Terms*—Cardiac action potential, FitzHugh-Nagumo equations, Maxwell's equations, Bioelectricity, Biomagnetism, Electrocardiography, Magnetocardiography.**

I. Introduction

The transverse current is the electric current flowing *orthogonal* to the longitudinal current $\hat{\sigma}\nabla\phi$ for a membrane potential ϕ and an anisotropic tensor $\hat{\sigma}$. This current has attracted widespread attention because the electric current that generates the magnetic field [3] [7] in the cardiac tissue is known to be orthogonal to $\hat{\sigma}\nabla\phi$, contrary to the previous longitudinal dipole hypothesis in which the magnetic current distribution is parallel to $\hat{\sigma}\nabla\phi$ [2] [31]. In the mathematical modeling of cardiac action potential propagation, the electric current density $\mathbf{J}$ has only been considered in the longitudinal direction $\hat{\sigma}\nabla\phi$, in what is known as the *longitudinal current hypothesis*. This hypothesis has been widely used together with Ohm's law for a static electric field $\mathbf{E} = -\nabla\phi$ to obtain [22] [28]

$$\mathbf{J} = \hat{\sigma}\mathbf{E} = -\hat{\sigma}\nabla\phi. \tag{1}$$

Thus, transverse current is intrinsically impossible in the monodomain model, although it can occur in the bidomain model if the conductivity tensor in the intracellular space, denoted by $\hat{\sigma}_i$, is obliquely oriented with respect to the conductivity tensor in the extracellular space, denoted by $\hat{\sigma}_e$. Then, the current density has the form $\mathbf{J} = -\hat{\sigma}_i\nabla\phi_i - \hat{\sigma}_e\nabla\phi_e$ as introduced by Roth and Woods to [32] represent the magnetic field in the cardiac action potential propagation. This bidomain model has been computationally tested and clinically adapted for the interpretation of electrocardiography (ECG) and magnetocardiography (MCG) [10] [17] [36] [38].

The author is with the Underwood International College, Yonsei University, South Korea, email: sehun.chun@yonsei.ac.kr, Webpage: https://sites.google.com/site/uicschun/. This work was initiated when the author stayed in AIMS South Africa.

However, the bidomain model of the transverse current sometimes results in erroneous regeneration of the existing magnetic field [10]. The problem is that the electric current is not purely orthogonal to $\hat{\sigma}\nabla\phi$, but can also be macroscopically parallel to $\hat{\sigma}\nabla\phi$. The present bidomain model of the transverse current fails to provide the observed broad distributions of the electric and pseudomagnetic currents far from the wavefront. Understanding three-dimensional geometric effect is also impossible. Moreover, it is problematic to use the Biot-Savart law to derive the magnetic field because the current may not be steady and one-dimensional and because the generated magnetic field does not affect the electric field or the membrane potential ϕ. Thus, it is necessary to address the question of how the magnetic field corresponding to cardiac excitation should be computed even in multidimensional space to explain the similarity of the patterns observed in ECG and MCG results?

In this paper, we propose a mathematical theory that can solve the above-mentioned issues. Thinking of the transverse current outside of the biologically unique bidomain structure poses problems in classical electrodynamics. Therefore, because biological problems are often treated as physical problems, macroscopic cardiac electrophysiological phenomena are herein considered in the context of classical electrodynamics. Such analysis can be performed by considering the dynamics of cardiac propagation without including the structure of the *cardiac tissue* through which the wave propagates, because the macroscopic propagation of an electromagnetic wave is often studied without considering its medium, known as the *aether* [37].

The theory proposed in this paper provides mathematical descriptions of bioelectricity in the context of biological electric current dynamics in the heart, but the descriptions can also be extended to bioelectromagnetics to incorporate the effects of external electromagnetic fields on cardiac action potential propagation. The main focus of this theory is on the organ size scale. The two-variable excitable media model, which is also called the *generic model* [6] [9], is used to describe the qualitative propagation behaviour efficiently. Thus, the proposed large-scale model of cardiac excitation propagation could be viewed as being oversimplified with respect to cellular-level modeling. However, this approach has many unique advantages. For example, this model can conveniently represent many multidimensional phenomena in the heart especially those related to three dimensional geometric effects on the electric current, such as fibrillation and defibrillation in the atria and ventricles, which is almost impossible to analyise in cellular-level modeling.

The objectives of this study were (i) to derive a set of

ISBN: 978-988-19253-0-5
ISSN: 2078-0958 (Print); ISSN: 2078-0966 (Online)
(revised on 1 June 2016)

Maxwell's equations equivalent to those in the generic two-variable model, (ii) to find a general expression for the transverse current even in the monodomain, (iii) to determine the fundamental mechanism that supplies the electric current that generates the magnetic field, and (iv) to validate the effect of the transverse current on the magnetic field in comparison with that of the longitudinal current.

This paper is organized as follows. Section 2 explains the differences between classical electrodynamics and the current electrophysiological mathematical model. Section 3 presents the derivation of the macroscopic Maxwell's equations. Section 4 describes the choice of gauge used to obtain the charge density and corresponding current density. The derived set of Maxwell's equations is shown, and its important properties are described in Section 5. Computational simulations for one-dimensional and two-dimensional spaces are presented in Sections 6 and 7, respectively. Discussion of the results immediately follows in Section 8.

II. Classical electrodynamics in cardiac excitation

When classical electrodynamics is applied to cardiac excitation, it must first to be noted is that the longitudinal current hypothesis of Eq. (1) is not electrodynamically correct. Cardiac excitation is not a static phenomenon, but rather a dynamic phenomenon in the sense that the electric charge contained in charged ions propagates. From the dynamic electric field equation $\mathbf{E} = -\nabla\phi - \partial\mathbf{A}/\partial t$, the current density can be written as

$$\mathbf{J} = \hat{\sigma}\mathbf{E} = -\hat{\sigma}\left(\nabla\phi + \frac{\partial\mathbf{A}}{\partial t}\right), \tag{2}$$

where $\mathbf{A}$ is the vector potential, which is defined as the curl of the magnetic field $\mathbf{B}$. In other words, $\mathbf{A} = \nabla \times \mathbf{B}$. Because $\partial\mathbf{A}/\partial t$ is not always aligned along the longitudinal direction $\hat{\sigma}\nabla\phi$, transverse current naturally occurs, even in the monodomain model, independent of the directions of $\hat{\sigma}_e$ and $\hat{\sigma}_i$.

TABLE I
Comparisons between the electromagnetic wave and the cardiac electric signal

	Electromagnetic wave	Cardiac excitation
Max. speed	$\approx 3.0 \times 10^8\ m/s$	$\approx 1.0\ m/s$
Medium	outer space	functional syncytium
Propagating object	photons	charged cations
Medium	electron	cardiac cell
Vacuum state	void of matter	cell in resting state

$\partial\mathbf{A}/\partial t$ has been disregarded in previous mathematical models of electrophysiology for several reasons. The strongest justification for its exclusion is provided by the experimental observation that cardiac electric signal propagation is significantly slower than electromagnetic wave propagation. The maximum electromagnetic wave speed is approximately $3 \times 10^8\ m/s$, but the cardiac signal speed is only about $1\ m/s$, even in an anisotropic medium [15]. This slow speed is often used to justify the so-called *quasi magnetostatic assumption* of biological phenomena in which $\mathbf{B} \approx 0$ approximately implies that $\partial\mathbf{A}/\partial t \approx 0$. This quasi-magneto static assumption has proven to be successful for many physical phenomena, even for cases in which the electromagnetic wave speed is significantly faster than the cardiac signal speed but notably slower than the speed of light. Consequently, in order to validate the claim that the dynamic version of Ohm's law (2) should be adopted instead of the static version (1), fundamental changes in cardiac electric signal propagation theory seems to be required.

The key point of this study was that the functional syncytium of cardiac tissues was considered as a *medium* that delivers electrical signals, rather than as a *dielectric material* that slows down electric waves. The propagation of electromagnetic waves on the macroscopic scale can be equivalently viewed as the continuous absorption and emission of photons on the quantum scale. The maximum electromagnetic wave speed is not an absolute constant, but rather is determined by the medium through which it is transmitted. Historically, this medium has often been called *aether* [37]. For example, in Maxwell's equations the maximum speed of light should be constant in a vacuum, but it does not have to be approximately $3.0\times10^8\ m/s$ unless the electromagnetic wave of interest propagates in outer space (Table I).

If the maximum speed of the electromagnetic wave speed for a cardiac electric signal is approximately $1.0\ m/s$, then the cardiac electric signal propagation through cardiac tissue can be considered as signal delivery by a different form of aether. This maximum speed differs by several orders of magnitude from the speeds observed experimentally for electromagnetic waves in the human body in the frequency range of $1 \sim 1000$ Hz, which have wavelengths of several kilometers [34]. However, the experimentally observed speeds have been measured by regarding cardiac tissue as a dielectric material, not a delivering aether. In this case, the resting state of cardiac tissue is the *vacuum* state, corresponding to the vacuum state in which electromagnetic waves travel at $3.0\times10^8\ m/s$. A cardiac signal's propagation speed can vary for many reasons, such as inhomogeneities in the media through which it propagates, wavefront curvature, and irregular pacing, but the signal's speed is not small compared to its maximum speed in the resting state.

If cardiac electric signal propagation is treated as the continuous absorption and emission of charged cations by the cardiac tissue in the resting state, the quasi-magneto static assumption is not valid, because the velocity is still close to the maximum speed of light in cardiac tissue in spite of the aforementioned factors that can cause propagation speed variations. Then, the derived electromagnetic fields and potentials induced in cardiac tissue do not necessarily are not qualitatively same as those of electromagnetic waves in outer space. Without using the quasi-magneto static assumption, an efficient method of modeling cardiac excitation propagation in multidimensional space iinvolves deriving the specific macroscopic Maxwell's equations for the dynamics of excitation propagation in cardiac tissue by choosing a gauge and electric sources.

III. From microscopic to macroscopic

Let π^i be the set of spatial locations occupied by myocardial cells, called the *intracellular space*. Let π^o be the space of the surrounding bath, called the *interstitial space*. π^i and π^o are microscopically separable with a distinctive boundary so that $\pi^i \cap \pi^o = \emptyset$. The membrane $\pi^i \cap \pi^o$ is considered to

ISBN: 978-988-19253-0-5
ISSN: 2078-0958 (Print); ISSN: 2078-0966 (Online)

be sufficiently thin so that every point in microscopic space belongs to either π^i or π^o.

A cardiac cell in the surrounding bath is roughly 100 μm long and 15 μm in diameter [15] [21]. If the microscopic scale is defined as the micrometer scale, then a domain consisting of a few cardiac cells is microscopic. Suppose that the microscopic domain (i) is statically continuous so that electric conductivity tensor is distributed smoothly and (ii) consists of only π^i and π^o, while other structures such as fibroblast can be neglected. For π^i and π^o, the microscopic Maxwell's equations can be written as

$$\begin{array}{ll} \nabla \cdot \mathbf{d}^k = \varrho^k, & \nabla \times \mathbf{e}^k = -\partial \mathbf{b}^k/\partial t, \\ \nabla \cdot \mathbf{b}^k = 0, & \nabla \times \mathbf{h}^k = \partial \mathbf{d}^k/\partial t + \mathbf{j}^k, \end{array} \tag{3}$$

where the superscripts k = 'i' and 'o' to indicate that the variable is defined in π^i and π^o, respectively. Let $\mathbf{e}$, $\mathbf{d}$, $\mathbf{h}$, $\mathbf{b}$ be the electric field, displacement field, h-field, and magnetic field, respectively, on the microscopic scale. ε_0 is the permittivity constant and μ_0 is the permeability constant for the resting state in which the electric signal speed is at its maximum of $c \approx 1\ m/s$, in which case $(\varepsilon_0^i \mu_0^i)^{-1/2} = (\varepsilon_0^o \mu_0^o)^{-1/2}$. ϱ is the charge density due to $\mathbf{d}$ and $\mathbf{j}$ is the current density corresponding to ϱ. Note that both ϱ^k and $\mathbf{j}^k$ are not trivial because of the transmembrane current between π^i and π^o. Even without an external energy source, charged ions transferred through the membrane have the same effects as a charge source would have on π^i and π^o [27] [28].

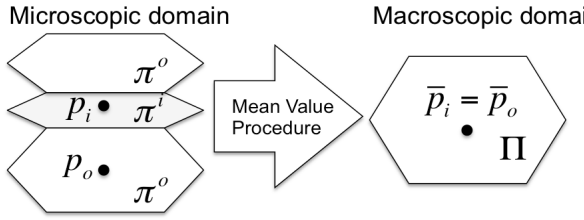

Fig. 1. From microscopic quantity p_i in π^i and p_o in π^o to macroscopic quantity $\bar{p}_i = \bar{p}_o$ in Π.

The shift from a microscopic quantity to a macroscopic quantity follows the mean value approach used by H. A. Lorentz [18] [25]. Relativistic transformation is not considered in this paper. The macroscopic scale is considered to be on the order of centimeters so that a domain that consists of hundreds or thousands of cardiac cells is macroscopic. For example, the macroscopic quantities $\mathbf{E}$ and ϕ can be obtained by averaging the integrals of the microscopic quantities $\mathbf{e}$ and φ: For the volume of a sphere V centered at each point in the microscopic domain

$$\mathbf{E} \equiv \frac{1}{V}\int \mathbf{e} dV, \qquad \phi \equiv \frac{1}{V}\int \varphi V.$$

The macroscopic components $(\mathbf{E}^i, \phi^i)$ are defined in the macroscopic domain Π^i that is constructed from π^i by increasing the size of the basic unit. Similarly, $(\mathbf{E}^o, \phi^o)$ is defined in Π^o. However, Π^i and Π^o are geometrically identical because a cardiac cell and its surrounding bath are indistinguishable on the macroscopic scale. Thus, $\Pi \equiv \Pi^o = \Pi^i$. One macroscopic point corresponds to microscopic points in both π^i and π^o. Consequently, each variable has two distinctive values at every macroscopic point. For example, for every point $p \in \Pi$, $(\mathbf{E}^i(p), \phi^i(p))$ coexists with $(\mathbf{E}^o(p), \phi^o(p))$, and they do not interfere with each other except at the membrane $\pi^i \cap \pi^o$. The charge density (ρ^i, ρ^o) and current density ($\mathbf{J}^i$, $\mathbf{J}^o$) can be similarly obtained. For rigorous mathematical derivations of the mean value procedure for Maxwell's equations by a smooth function with a compact support, refer to ref. [34].

Based on the dielectric properties of cardiac tissue, suppose that the magnetic field $\mathbf{B}$ has a constant linear constitutive relationship with the $\mathbf{H}$-field that is given by $\mathbf{B} = \mu_0 \mathbf{H}$ without magnetic polarization, as assumed in ref. [34]. On the other hand, suppose that the displacement field $\mathbf{D}$ has a tensor relationship with $\mathbf{E}$ that includes the electric polarization density $\mathbf{P}$ and can be expressed as

$$\mathbf{D} = \hat{\varepsilon}\mathbf{E} + \mathbf{P}, \qquad \text{where} \quad \hat{\varepsilon} = \varepsilon_0 \hat{I} + \frac{\hat{\sigma}}{i\omega}, \tag{4}$$

where $i = \sqrt{-1}$, ω is the wave frequency, and $\hat{I}$ is the unit tensor. The construction of $\hat{\varepsilon}$ reflects the structure of cardiac tissue, in which the conductivity $\hat{\sigma}$ is anisotropic and the permittivity $(\varepsilon_0 \hat{I})$ is homogeneous and isotropic.

Because all of the fields and variables are in the same macroscopic domain Π, the macroscopic Maxwell's equations for π^i can be subtracted from those for π^o (3) to obtain

$$\nabla \cdot \hat{\sigma}\mathbf{E} = \rho_e, \quad \nabla \times \mathbf{E} = -\frac{\partial \mathbf{B}}{\partial t}, \tag{5}$$

$$\nabla \cdot \mathbf{B} = 0, \quad \nabla \times \mathbf{H} = \varepsilon_0 \frac{\partial \mathbf{E}}{\partial t} + \hat{\sigma}\mathbf{E} + \mathbf{J}_e, \tag{6}$$

where ρ_e is the charge density due to $\hat{\sigma}\mathbf{E}$, and $\mathbf{J}_e$ is the current density corresponding to ρ_e that satisifies $\mathbf{J}_e = \mathbf{J} + \partial \mathbf{P}/\partial t$, which can be obtained from the equality $\nabla \cdot \hat{\sigma}\mathbf{E} = \nabla \cdot \hat{\varepsilon}\mathbf{E}$. The new macroscopic fields and potentials are defined by the differences between the two quantities in π^i and π^o. The above Maxwell's equations (5) and (6) cannot determine the electromagnetic field because ρ_e and $\mathbf{J}_e$ are unknown. In the following section, ρ_e and $\mathbf{J}_e$ are chosen accordingly so that the macroscopic Maxwell's equations (5) and (6) also represent the dynamics of the two-variable excitable media model of cardiac electric signal propagation.

IV. Deriving ρ_e and $\mathbf{J}_e$

By applying a sufficiently smooth and differentiable conductivity tensor $\hat{\sigma}$ and the divergence operator to the expression of the dynamic electric field expression, we can obtain

$$-\frac{\partial(\nabla \cdot \hat{\sigma}\mathbf{A})}{\partial t} = \nabla \cdot \hat{\sigma}\nabla\phi + \rho_e. \tag{7}$$

In electromagnetics, $\nabla \cdot \mathbf{A}$ is called the *gauge choice* and can be chosen randomly, although it is widely considered that the gauge choice should reflect the subatomic excitation mechanism of the signal oscillator, as do the Coulomb and Lorentz gauges for classical electrodynamic waves [18] [19]. For the electrodynamics of cardiac action potential propagation, a new gauge is proposed:

$$\nabla \cdot (\hat{\sigma}\mathbf{A}) = -\phi. \tag{8}$$

The meaning of the gauge choice (8) can be briefly explained as follows. Consider an isotropic domain $\Omega \in \Pi$.

ISBN: 978-988-19253-0-5
ISSN: 2078-0958 (Print); ISSN: 2078-0966 (Online)

Combining Eq. (7) with Eq. (8) and the divergence theorem yields

$$\int_\Omega \frac{\partial(\nabla\cdot\mathbf{A})}{\partial t}dx - \int_{\partial\Omega}\nabla\phi\cdot\mathbf{n}dS = \int_\Omega \rho_e dx,$$

where $\mathbf{n}$ is the normal vector of the boundary $\partial\Omega$. The first component is zero for the Coulomb gauge and is also negligible for the Lorentz gauge when ϕ varies sufficiently smoothly. However, the first component is not trivial for our gauge choice (8). The total charge can also be modified by the time variation of ϕ, not just by the flux caused by the gradient of ϕ through the boundary. Therefore, any new energy source in the medium, such as the membrane current expressed as $d\phi/dt$ in the mathematical model, contributes to the changes in the total charge and, eventually, in the electromagnetic field.

In fact, this gauge plays an important role in monodomain and bidomain equations. If the dynamic electric field of Eq. (2) is used instead of the static electric field of Eq. (1) to determine the current density, then the monodomain equation is modified becomes

$$\frac{\partial\phi}{\partial t} = \nabla\cdot\hat{\sigma}\nabla\phi + \frac{\nabla\cdot(\hat{\sigma}\mathbf{A})}{\partial t} + I_{ion}.$$

The gauge choice (8) preserves the form of the diffusion-reaction for cardiac excitation propagation, and the dynamic electric field produces a model qualitatively identical to that produced by the static electric field. This preservation is also true for the Coulomb gauge, but not for the Lorentz gauge. By directly applying calculus and the conservation of charge, $\mathbf{J}_e$ that is expressed as $-i\mathbf{k}/k^2\dot{\rho}_e\hat{\sigma}^{-1}$ in the reciprocal space is equivalently expressed in the physical space as

$$\mathbf{J}_e = -\frac{\varepsilon_0}{4\pi}\int \dot{\rho}_e(r')\hat{\sigma}^{-1}\frac{\mathbf{r}-\mathbf{r}'}{|\mathbf{r}-\mathbf{r}'|^3}d^3r' - \hat{\sigma}\mathbf{E}, \qquad (9)$$

where the dot indicates the time derivative. The values of ρ_e and $\dot{\rho}_e$ in two popular models are displayed in Table II. $\mathbf{J}_e$ can be computed by solving $\nabla\cdot\hat{\sigma}\mathbf{J}_e = -\dot{\rho}_e$ or a Poisson equation such as $\mathbf{J}_e = -\hat{\sigma}\nabla\phi_s$ where the new potential ϕ_s, called the *reaction potential*, satisfies $\nabla\cdot\hat{\sigma}\nabla\phi_s = \dot{\rho}_e$. The latter method is employed in this paper for simplicity.

The physiological meaning of $\mathbf{J}_e$ can be elucidated by using a simple FitzHugh Nagumo model. Consider $\rho_e = \phi - \phi^3/3 - \psi$ and $\dot{\psi} = \phi - \psi$ [13] [14] [26]. Then, $\mathbf{J}_e$ is given by

$$\mathbf{J}_e = \frac{\partial\hat{\sigma}\mathbf{A}}{\partial t} + \frac{\varepsilon_0}{4\pi}\int \phi^2(r')\left[\dot{\phi}(r') + \frac{\phi(r')}{3}\right]\frac{\mathbf{r}-\mathbf{r}'}{|\mathbf{r}-\mathbf{r}'|^3}d^3r'.$$

The first component is the difference between $\sigma\mathbf{E}$ and $-\hat{\sigma}\nabla\phi$ and is equal to the difference between the dynamic and static electric fields. The second component is the additional source with a magnitude of $\phi^2(\dot{\phi} + \phi/3)$ that is caused by the membrane current. Because $\mathbf{J_e} = \mathbf{J} + \partial\mathbf{P}/\partial t$, the electric polarization in the electrodynamics of cardiac excitation represents the current density change that is caused by the membrane current. In other words, the additional membrane current source can be expressed as the *electric polarization* in the derived Maxwell's equations, similarly to how it would be expressed in classical electrodynamics and bioelectromagnetics [34].

V. Electromagnetic model of cardiac excitation

The previous derivations can be briefly summarized by the following proposition.

Proposition 1: In a macroscopic domain Π, the general two variable monodomain model

$$\frac{\partial\phi}{\partial t} = \nabla\cdot\hat{\sigma}\nabla\phi + \rho_e(\phi,\psi), \qquad (10)$$

$$\frac{\partial\psi}{\partial t} = G(\phi,\psi) \qquad (11)$$

is equivalent to the Maxwell's equations

$$\nabla\times\mathbf{E} = -\frac{\partial\mathbf{B}}{\partial t}, \qquad (12)$$

$$\nabla\times\mathbf{H} = \frac{\partial\mathbf{E}}{\partial t} + \nabla\phi_s, \qquad (13)$$

where the reaction potential ϕ_s is the solution of the Poisson equation $\nabla\cdot\hat{\sigma}\nabla\phi_s = \dot{\rho}_e$. Thus, the second term in Eq. (13) can be regarded a *gravitational field* being caused by $\dot{\rho}_e$.

The above proposition implies that the cardiac electric signal propagation can also be modeled as field equations that are invariant under Lorentz transformation. Because $\nabla\phi_s$, representing the macroscopic current caused by the membrane current, can be considered as an electric current, the above equations (12) and (13) can be combined with Eqs. (5) and (6) and expressed as

$$\partial_\alpha F^{\alpha\beta} = J^\beta, \qquad \partial_{[\alpha}F_{\beta\gamma]} = 0,$$

where $F^{\alpha\beta}$ and J^α are the electromagnetic field tensor and the 4-current, respectively. Thus, the Lagrangian density is the same and consequently the fundamental equations describing the particle dynamics should be the same. However, the macroscopic cardiac excitation propagation mechanism is not necessarily exactly the same as that of electromagnetic waves, because the general properties of the medium, i.e., cardiac tissue, are not the same as those of a vacuum, as expressed in the constitution equation Eq. (4).

The medium through which the electric signal is transmitted can be categorized according to the following properties [29]: (1) nonlinearity, (2) dissipativity, (3) isotropy, (4) reciprocality, (5) uniformity, and (6) dispersiveness. These properties are well expressed by the real and imaginary components of the permittivity and permeability. Each of these properties is significantly different for a vacuum and cardiac tissue.

1) **Nonlinearity and dissipativity** The strong nonlinearity of cardiac electric signal propagation causes energy degradation due to dissipation. Nonlinearity is related to the imaginary component of permittivity, i.e., the conductivity tensor.
2) **Anisotropy**: Another unique characteristic of cardiac tissue is its strong anisotropy. The ratio of the propagational velocities along the fiber, sheet, and normal direction can be as large as 4:2:1 [39]. However, unlike in electrodynamic anisotropic phenomena such as birefringence and natural optical activity, the anisotropic propagation is expressed by the conductivity tensor, rather than by the anisotropic real component of the permittivity tensor.
3) **Reciprocality**: The most well-known non-reciprocal properties of electromagnetic waves are the consistency

ISBN: 978-988-19253-0-5
ISSN: 2078-0958 (Print); ISSN: 2078-0966 (Online)

of the speed of light even in a moving medium, known as the *Fresnel Fizeau effect*, and the dielectric and magnetic rotation of the polarization plane, known as the *Faraday effect*. The existence of the same reciprocality in cardiac tissue is not known, but other reciprocalities, such as (i) one-way propagation (ii) the absence of any significant reflected waves, and (iii) the lack of wave superposition, have been clinically observed and studied in the cardiology community. These phenomena are all related to the existence of a refractory area that results in nonsymmetric propagation in space and time.

The unique propagation mechanism in the cardiac tissue can also be explained by the current density $\nabla\phi_s$ which depends on the temporal and spatial variations. If ρ_e is constant in time or in space, then Maxwell's equations (12) and (13) are under conservation laws without any additional energy source. The additional charge source, i.e., the membrane current, is present when the distribution of ρ_e is nonuniform in space and time. If $\dot{\rho}_e > 0$, then the presence of $\dot{\rho}_e$ corresponds to a medium with a *source* that contributes additional charge. If $\dot{\rho}_e < 0$, then the presence of $\dot{\rho}_e$ corresponds to a medium with a *sink* that decreases the charge. This mathematical deduction is consistent with biological effects of the membrane current that is physiologically achieved by ion channels, ion pumps, and exchanger current.

In the following sections, to relate the distribution of the electromagnetic field to the propagation of the membrane potential ϕ in one- and two-dimensional space, numerical solutions to Maxwell's equations (12) and (13) are presented. For detailed numerical schemes and convergence tests, see Appendix A.

VI. 1D Propagation

Consider a one-dimensional domain of length 500 (which corresponds to a real length of approximately $50\ cm$), and let the cardiac electric signal propagate from the left wall at $x = 0$. Two monodomain models are considered: the FitzHugh Nagumo model and the Rogers McCulloch model. Only the former has a hyperpolarization period in which the membrane potential ϕ is below its value in the resting state. The values of ρ and $\dot{\rho}$ are displayed in Table II.

In Fig. 2, to the distributions of ϕ and ψ (first row), the electromagnetic field $(\mathbf{E}, \mathbf{B})$ (second row), the displacement field and the vector potential $(\mathbf{D}, \mathbf{A})$ (third row), and the reaction potential and the time rate change of reaction $(\phi_s, \dot{\rho}_e)$ (last row) are displayed in both of the aforementioned models. Contrary to the Gaussian-like distributions of ϕ and ψ with a compact support, the electric field $\mathbf{E}$ is immediately affected by the instantaneous force term $\dot{\rho}_e$ of the Poisson equation (17) and is distributed smoothly throughout the domain. However, the magnetic field $\mathbf{B}$ remains zero for one-dimensional propagation. The shape of the displacement field is similar to that of the membrane potential, which implies that the signal propagates in form of the electric field and the electric polarization. The fact that the maximum magnitude of the vector potential $\mathbf{A}$ occurs near the action potential suggests the maximum absorption and emission also occur in that region, which is physiologically true. The reaction

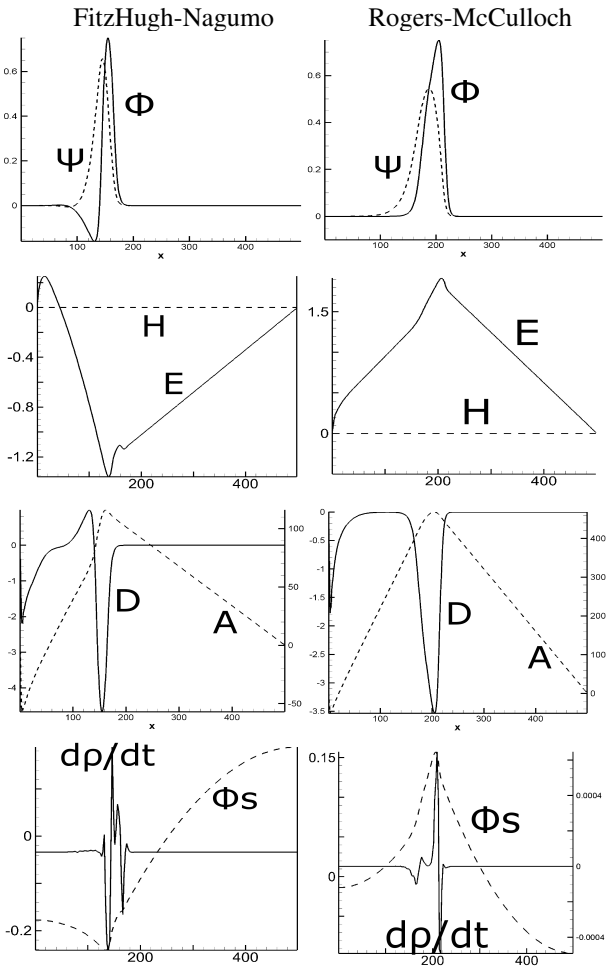

Fig. 2. One-dimensional distribution of the potentials and fields for the original FitzHugh-Nagumo model and the Rogers-McCulloch model.

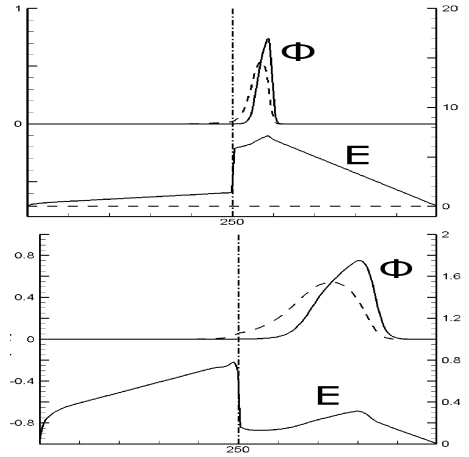

Fig. 3. One-dimensional distribution of $(\phi(|), \psi(:))$ and $(E(|), B(:))$ when $\sigma_x = 0.25$ (top) and $\sigma_x = 4.0$ (bottom) for $x > 250$.

potential ϕ_s is distributed smoothly according to the force distribution of the almost point-wise charge $\dot{\rho}_e$.

The propagation of $\mathbf{E}$ is directly affected by the electric conductivity $\hat{\sigma}$, because the source of $\mathbf{E}$ is the gradient of the reaction potential ϕ_s and because the reaction potential ϕ depends on $\hat{\sigma}$. This phenomenon is verified by Fig. 3. The magnitude of $\mathbf{E}$ is approximately inversely proportional to the magnitude of $\hat{\sigma}$.

In the collision of multiple cardiac waves, the principle of

ISBN: 978-988-19253-0-5
ISSN: 2078-0958 (Print); ISSN: 2078-0966 (Online)

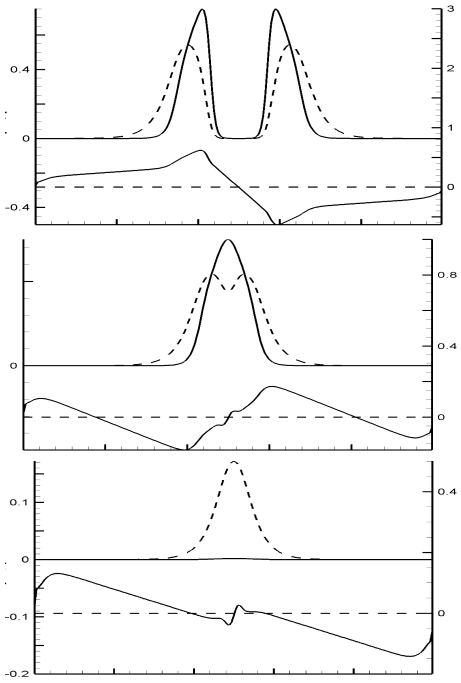

Fig. 4. Collision of two cardiac excitations at $T = 800$ (top), $T = 1000$ (middle), and $T = 1300$ (bottom). Upper lines in each plot are $(\phi(|), \psi(:))$ and lower lines are $(\mathbf{E}(|), \mathbf{B}(:))$. $T = 1$ corresponds to 0.63 ms.

superposition was previously thought to be violated, causing the propagation to be nonlinear. However, the principle of superposition can be applied to explain the collision of cardiac waves. The time-series field distribution for the collision of two cardiac waves is displayed in Fig. 4, in which waves that are initiated at the ends propagate towards one another and meet in the middle. As soon as the two humps of ϕ merge into a single hump at a computational time T of 1200, the reaction potential ϕ_s for $\mathbf{E}$ becomes a smooth Gaussian curve and loses its sharp gradient. This change indicates that the source of $\mathbf{E}$ is significantly weakened and becomes negligible. Nevertheless, the sink remains active independent of ϕ. Thus, $\mathbf{E}$ diminishes as it travels further into the tail end of the other wave. Moreover, $\mathbf{E}$ in the backside of the other wave has a magnitude similar to that of the diminishing $\mathbf{E}$, but the opposite sign. Therefore, the total $\mathbf{E}$, which is the sum of the diminishing $\mathbf{E}$ and the backside $\mathbf{E}$, becomes zero, and the wave is annihilated (at $T > 1300$) according to the principle of superposition.

VII. Two-dimensional propagation

For two-dimensional modeling, the transverse electric (TE) mode was chosen considering the anisotropy of the electric conductivity in cardiac tissue.

A. Isotropic plane

Consider a two-dimensional square of length 100 (equivalent to a real length of 10 cm). Let the propagation be circularly initiated from the top left corner in the isotropic medium with $\hat{\sigma} = \hat{I}$. Fig. 5 displays the distribution of vector field distribution corresponding to ϕ at computational time $T = 500$ (equivalent to a real time of 0.32 s). The electric field $\mathbf{E}$ is in the same direction as the displacement field $\mathbf{D}$. Bu,t the main difference is that the electric field is distributed

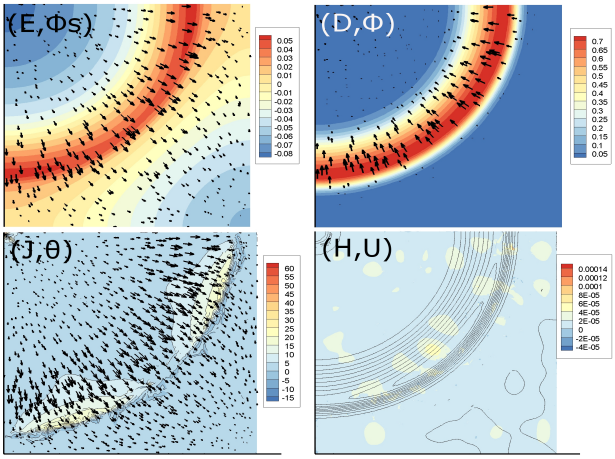

Fig. 5. Isotropic plane with $\hat{\sigma} = \hat{I}$. Vector variables ($\mathbf{E}$, $\mathbf{D}$, $\mathbf{A}$, $\mathbf{J}$) by arrows and scalar variables (ϕ_s, ϕH_z, θ) by colour. θ is the angle between $\mathbf{J}$ and $\mathbf{D}$. The lines represent the isopotential contour of ϕ.

over a larger area including the depolarizing area, whereas the displacement field is mostly not trivial in the depolarizing area. The (J, θ) plot displays the angular difference between $\mathbf{E}$ and $\mathbf{D}$ that is mostly significant especially along the wavefront.

The yellow region in the (J, θ) plot of Fig. 5 displays this transverse current corresponding to the transverse component of $\mathbf{E}$. Only in the yellow region, the current density $\mathbf{J}$ has an angle of approximately 30° with respect to the displacement field $\mathbf{D}$. In the yellow region, the direction of $\mathbf{E}$ changes dramatically, so $\nabla \times \mathbf{E}$ is not zero. Therefore, a magnetic field is generated in the yellow region according to Faraday's law (Eq. (12)), as shown in the (A, H_z) plot of Fig. 5. The existence of a magnetic field in the absence of a cardiac fiber $\hat{\sigma}$, although its magnitude remains relatively weak, was not predicted by the previous bidomain model.

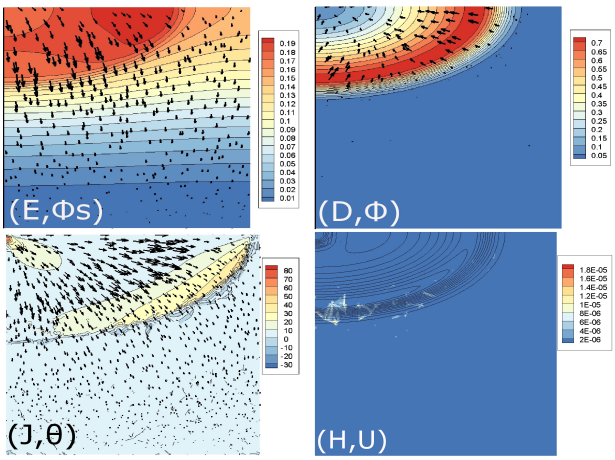

Fig. 6. Plane with straight anisotropy $\hat{\sigma} = 4\hat{x} + \hat{y}$. Vector variables ($\mathbf{E}$, $\mathbf{A}$, $\mathbf{J}$) by arrows and scalar variables (ϕ_s, H_z, θ, U) by colour. θ is the angle between $\mathbf{J}$ and $\mathbf{D}$. The lines represent the isopotential contour of ϕ.

B. Anisotropic plane with straight cardiac fibre

Consider the same plane with the cardiac fiber aligned along the x-axis, as was used in ref. [17]. Then, the conductivity tensor can be expressed as $\hat{\sigma} = 4\hat{x} + \hat{y}$. Suppose that the propagation is initiated point-wise in the top-left corner,

ISBN: 978-988-19253-0-5
ISSN: 2078-0958 (Print); ISSN: 2078-0966 (Online)
(revised on 1 June 2016)

at $(x, y) = (-75, 75)$. In this case, the direction of $\mathbf{E}$ differs significantly from that of $\mathbf{D}$, especially in the depolarizing zone where the propagation occurs along the fibre direction. This difference is a direct consequence of the fact that the contour of ϕ is not coincident with the contour of ϕ_s. The area in which the angle between $\mathbf{J}$ and $\mathbf{D}$ is larger than 40° is significantly broader than that for the isotropic plane, as indicated by the yellow region in the (J, θ) plot of Fig. 6. Consequently, the magnetic field emerges in a broader region near the wavefront, as shown in the (A, H_z) plot of Fig. 6.

Comparison of this result with Fig. 4 of ref. [17] confirms that the magnetic field is aligned along the wavefront of the cardiac action potential. However, the (J, θ) plot of Fig. 6 shows that the transverse current only appears in the yellow area. This observation is in contrast to the previous claim that a pure transverse current $\mathbf{J}$ only induces a magnetic field in [17]. It was suggested in ref. [11] that the existence of a pure transverse current is questionable because there are multiple interpretations of the magnetic field created by the longitudinal current along a cardiac fiber.

Another important characteristic of in Fig. 6 is that the magnetic field depends on the angle between $\mathbf{J}$ and $\hat{\sigma}$. In the left part of the wavefront, the direction of $\mathbf{J}$ slowly shifts toward the orange region in the repolarization zone to form an oblique angle with the cardiac fiber $\hat{\sigma}$ where the magnetic field is generated. However, in the right part of the wavefront, the direction of $\mathbf{J}$ remains along the x-direction, parallel to the cardiac fiber, and the magnetic field is negligible as shown in the (A, H_z) plot of Fig. 6. This observation confirms the prediction of the previous bidomain model that the magnetic field depends on the angle between the current density flow and the cardiac fiber [32].

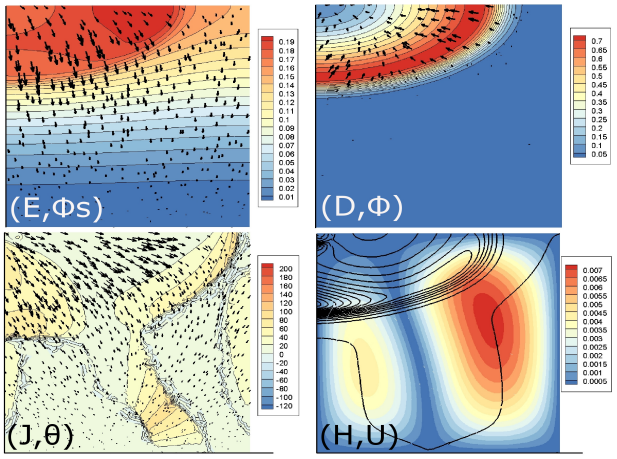

Fig. 7. Plane with circular anisotropy $\hat{\sigma} = 4\hat{\theta} + \hat{r}$ where $r^2 = x^2 + (y+120)^2$. Vector variables ($\mathbf{E}$, $\mathbf{A}$, $\mathbf{J}$) by arrows and scalar variables (ϕ_s, H_z, θ) by colour. θ is the angle between $\mathbf{J}$ and $\mathbf{D}$. The lines represent the isopotential contour of ϕ.

C. Anisotropic plane with circular fiber

The proposed electrodynamic model also demonstrates that it is possible for the magnetic field to appear in regions far from the wavefront. Consider a circularly anisotropic plane centered at $(0, -120)$ in the same domain so that the conductivity tensor can be defined as $\hat{\sigma} = 4\hat{\theta} + \hat{r}$, where $r^2 = x^2 + (y + 120)^2$.

In Fig. 7, the distributions of ϕ, $\mathbf{E}$, $\mathbf{D}$ are similar to those for the linearly anisotropic fiber $\hat{\sigma} = 4\hat{x} + \hat{y}$. However, the distribution of $\mathbf{J}$ differs significantly, mainly due to the change in the distribution of ϕ_s that is caused by the different direction of the circularly-distributed cardiac fiber. This change can be observed by comparing the (J, θ) plots of Figs. 6 and Fig. 7. Consequently, a significant amount of the magnetic field is generated for the circular fibre in a large area far from the depolarization zone, as shown in the (H, U) plot of Fig. 7. However, the different distribution of the magnetic field does not directly imply the different distribution of $\nabla \times \mathbf{J}$ for the current source for the magnetic field according to the Biot-Savart equation.

Fig. 8 displays the distributions of $\nabla \times \mathbf{J}$, which is the magnetic field source, and the Poynting vector $\mathbf{S}$, which is defined by $\mathbf{S} \equiv (1/\mu_0)\mathbf{E} \times \mathbf{B}$, to represent the energy flux density. Both plots shows the distribution of $\nabla \times \mathbf{J}$ is along the wavefront independent of the cardiac fibre direction and the magnetic field. Consequently, using the Biot-Savart equation should yield the same distribution of the magnetic field, which contradicts our simulation. This is because $\nabla \times \mathbf{J}$ is not a one-dimensional line segment in the two-dimensional space; in principle the magnetic field should be computed as a field variable from the electric field. The different magnitude and direction of the Poynting vector demonstrates the different directional energy flows caused by the different magnetic field. This model explains the broad distribution of the magnetic field, including the separation of the axis of the MCG results from the wavefront, which has been conjected to be caused by the longitudinal dipole hypothesis [10].

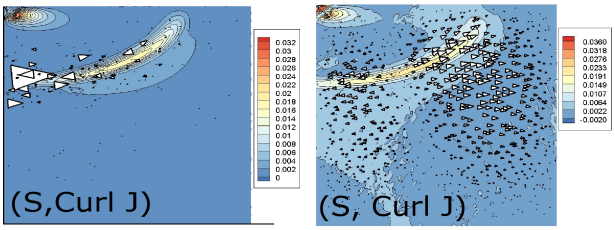

Fig. 8. Distribution of the Poynting vector ($\mathbf{S}$) (arrow) and $\nabla \times \mathbf{J}$ (colour contour) for the straight cardiac fibre ($\hat{\sigma} = 4\hat{x} + \hat{y}$) (left) and the circular cardiac fibre ($\hat{\sigma} = 4\hat{\theta} + \hat{r}$) (right). The lines represent the contour of the membrane potential ϕ.

VIII. Discussion

In the electromagnetic field theory of cardiac electric signal propagation, the transverse current induces the magnetic field because the transverse current causes dramatic changes in the electric current, while the longitudinal current is everywhere. The transverse current causes $\nabla \times \mathbf{J}$ to be nontrivial, and a magnetic field is consequently generated according to Faraday's law, not the Biot-Savart law. However, a non-negligible transverse current is not a necessary and sufficient condition for a magnetic field to exist.

Furthermore, the magnetic field does not have to appear only along the wavefront; instead, it may appear in other regions depending on the electric current propagation and the cardiac fiber direction. The correlation between the transverse current and the magnetic field is generally weak, but it could be strong for certain geometric alignments of the cardiac fiber. Nevertheless, it is true that the magnetic field

ISBN: 978-988-19253-0-5
ISSN: 2078-0958 (Print); ISSN: 2078-0966 (Online)

$\mathbf{H}$ in Eqs. (12) and (13) may not be the same as the magnetic field from the source of $\nabla \times \mathbf{J}$ as detected by MCG. In other word, the former magnetic field exists in the cardiac media and the latter magnetic field exists in the space. We assume that these two magnetic fields are strongly correlated, which may not be true in reality.

The disadvantages of this electromagnetic field theory are as follows. (i) The computational cost of evaluating $(\mathbf{E}, \mathbf{B})$ is higher than that of solving the diffusion-reaction equations. In addition to the diffusion-reaction equations, Maxwell's equations and one Poisson equation should be solved for each time step. The additional cost increases quadratically with dimensions. (ii) The electromagnetic model inherits most of the drawbacks of general two-variable excitable models [5] [6] [9] [24]. However, the electromagnetic model can also be combined with other cell models, such as the Luo-Rudy model [33]

One benefit that compensates for the large computational cost or the proposed model is the fundamental information that it yields about complex cardiac electrophysiological phenomena that could not be obtained by using two-variable diffusion-reaction equations on the macroscopic scale. It could yield many tools that would be useful for mathematical studies, such as geometric interpretations of propagation trajectories, Lagrangian and Hamiltonian approaches, and simpler Eikonal equations. The electric current can easily be computed from the electric field, and the magnetic field can be displayed to facilitate the analysis of MCG results. The energy flux and density can be used to understand the flow of charged ions in cardiac tissue. The geometric model of cardiac restitution and the bioelectromagnetics of defibrillation will be studied from the perspective of electrodynamics in the near future [4] [12] [40] [41].

APPENDIX

In a two-dimensional plane Ω, let $\mathbf{E} = E_x\mathbf{x} + E_y\mathbf{y}$ and $H_z = \mathbf{H} \cdot \mathbf{z}$. Then, the TE mode of (12) and (13) can be written in a normalized form such as

$$\frac{\partial E_x}{\partial t} = \frac{\partial H_z}{\partial y} - \frac{\partial \phi_s}{\partial x}, \tag{14}$$

$$\frac{\partial E_y}{\partial t} = -\frac{\partial H_z}{\partial x} - \frac{\partial \phi_s}{\partial y}, \tag{15}$$

$$\frac{\partial H_z}{\partial t} = \frac{\partial E_x}{\partial y} - \frac{\partial E_y}{\partial x}, \tag{16}$$

where the reaction potential ϕ_s is the solution of the Poisson solver

$$\frac{\partial}{\partial x}\left(\sigma_x \frac{\partial \phi_s}{\partial x}\right) + \frac{\partial}{\partial y}\left(\sigma_y \frac{\partial \phi_s}{\partial y}\right) = \dot{\rho}_e(\phi, \psi) - \int_\Omega \dot{\rho}_e dx. \tag{17}$$

with the pure Neumann boundary conditions such that

$$\frac{\partial \mathbf{E}}{\partial n} = 0, \quad \frac{\partial H_z}{\partial n} = 0, \quad \frac{\partial \phi}{\partial n} = 0, \quad \frac{\partial \phi_s}{\partial n} = 0, \quad \text{on } \partial\Omega, \tag{18}$$

where n is a parameter in the direction of the edge normal vector on $\partial\Omega$. Note that ρ_e is a function of $\phi(x, y, t)$ and $\psi(x, y, t)$, which are updated by solving the diffusion-reaction equations (10) and (11). To obtain effective solutions, the average of the force term in the Poisson equation can be made zero by adding $-\int_\Omega \dot{\rho}_e dx$. ϕ_s is not unique and in fact can have infinitely many values because it includes an arbitrary constant, but it does not affect the uniqueness of E_x and E_y because only the gradient of ϕ_s is used. Moreover, to compare the longitudinal flow with the transverse flow, the displacement field $\mathbf{D}$ must also be computed, by using

$$\frac{\partial D_x}{\partial t} = \frac{\partial H_z}{\partial y} - \sigma_x \frac{\partial \phi}{\partial x}, \tag{19}$$

$$\frac{\partial D_y}{\partial t} = -\frac{\partial H_z}{\partial x} - \sigma_y \frac{\partial \phi}{\partial y}. \tag{20}$$

For the computational simulations, the above equations were solved in the context of the discontinuous Galerkin (DG) method. The computational code was implemented in `nektar++`, a `C++` object-oriented spectral/hp library [35]. For the numerical flux, the upwind flux was used for Maxwell's equations [16] and conservation laws [20]. Also, the hybrid flux [23] was used for the diffusion-reaction equations (10) - (11) and the Poisson equation (17). For the time integration, the implicit explicit (IMEX) Runge Kutta third-order scheme was used in order to increase the maximum size of stable time step size, which was strongly restricted by the elliptic operator. For the maximum edge length of 10.0, a time step of 0.1 was used. Moreover, to represent the anisotropic conductivity tensor efficiently with different orientations, the method of moving frames was employed [8]. All of the computations were performed on a Macbook Pro personal laptop with 4GB of memory. The actual program contained 11 variables (E_x, E_y, H_z, D_x, D_y, A_x, A_y, ϕ, ψ, ϕ_s), but all of the computations presented in this paper were obtained in less than half a day of computation time.

Any charge density ρ_e and G in (10) could be used, provided that they accurately represent the cardiac excitation propagation accurately. In this study, their values were adapted from the Rogers McCulloch model [30], unless stated otherwise. However, other generic two-variable models such as the Aliev Panfilov model [1] are expected to produce qualitatively similar results.

The numerical scheme for the above equations was tested by considering the domai $\Omega(x, y) = [-1, 1] \times [-1, 1]$ and an arbitrary conductivity tensor $\hat{\sigma} = \sigma_x\mathbf{x} + \sigma_y\mathbf{y}$, in which case the following functions are the exact solutions of Eqs. (14) - (18):

$$\begin{aligned}
\phi &= \cos\pi x \cos\pi y \cos\omega t, \\
\phi_s &= (\omega \sin\omega t + \cos\omega t)\cos\pi x \cos\pi y, \\
\rho_e &= \pi^2(\sigma_x + \sigma_y)\cos\pi x \cos\pi y \cos\omega t - \omega \cos\pi x \cos\pi y \sin\omega t, \\
E_x &= \frac{1}{\sqrt{2}} \sin\pi x \cos\pi y((1-\omega)\cos\omega t + \sin\omega t), \\
E_y &= \frac{1}{\sqrt{2}} \cos\pi x \sin\pi y(-(1+\omega)\cos\omega t + \sin\omega t), \\
H_z &= -\sin\pi x \sin\pi y \sin\omega t,
\end{aligned}$$

where $\omega = \sqrt{2}\pi$. In Fig. (9), plots of the spectral L_2 convergence versus the polynomial order p are displayed for the isotropic case, in which $\sigma_x = 1$ for all x, and for the anisotropic case, in which $\sigma_x = 4$ for $x \geq 0$ and $\sigma_x = 1$ otherwise. For both cases, $\sigma_y = 1$ for all x.

ISBN: 978-988-19253-0-5
ISSN: 2078-0958 (Print); ISSN: 2078-0966 (Online)

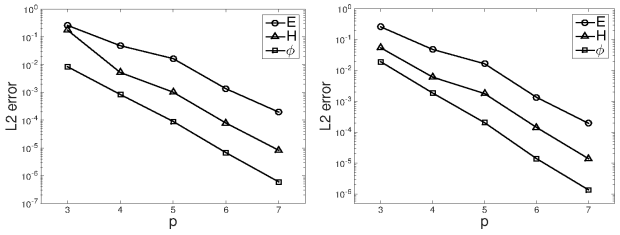

Fig. 9. Spectral L_2 convergence of the test problem for $\sigma_x = 1$ for all x (left) and $\sigma_x = 4$ for $x \geq 0$ and $\sigma_x = 1$ otherwise. For both cases, $\sigma_y = 1$ for all x.

TABLE II
FITZHUGH-NAGUMO:
$a = 0.12, b = 0.011, c_1 = 0.175, c_2 = 0.03, d = 0.55.$
ROGERS-MCCULLOCH:
$a = 0.13, b = 0.013, c_1 = 0.26, c_2 = 0.1, d = 1.0$ [30].
$c_\phi = -3c_1\phi^2 + 2(c_1(a+1))\phi - ac_1$

	$\rho_e, \dot{\rho}_e, \dot{\psi}$
FitzHugh-Nagumo	$\rho_e = c_1\phi(\phi - a)(1 - \phi) - c_2\psi$ $\dot{\rho}_e = c_\phi\dot{\phi} - c_2\dot{\psi}$ $\dot{\psi} = b(\phi - d\psi)$
Rogers-McCulloch	$\rho_e = c_1\phi(\phi - a)(1 - \phi) - c_2\phi\psi$ $\dot{\rho}_e = c_\phi\dot{\phi} - c_2(\dot{\phi}\psi + \phi\dot{\psi})$ $\dot{\psi} = b(\phi - d\psi)$

REFERENCES

[1] R. R. ALIEV AND A. V. PANFILOV, *A simple two-variable model of cardiac excitation*, Chaos, Solitons and Fractals, 7 (1996), pp. 293–301.

[2] J. BARACH, *A simulation of cardiac action currents having curl*, IEEE Trans. on Biomed. Eng., 40 (1993), pp. 49–58.

[3] G. M. BAULE AND R. MCFEE, *Detection of the magnetic field of the heart*, Amer. Heart J., 66 (1963), pp. 95–96.

[4] C. S. BECK, W. H. PRITCHARD, AND H. S. FEIL, *Ventricular fibrillation of long duration abolished by electric shock*, J. Amer. Medi. Asso., 135 (1947), pp. 985–986.

[5] V. N. BIKTASHEV, *Dissipation of the excitation wave fronts*, Phys. Rev. Lett., 89 (2002), p. 168102.

[6] V. N. BIKTASHEV, R. SUCKLEY, Y. E. ELKIN, AND R. D. SIMITEV, *Asymptotic analysis and analytical solutions of a model of cardiac excitation*, Bull. Math. Biol., 70 (2008), pp. 517–554.

[7] D. BURSTEIN AND D. COHEN, *Comparison of magnetic field and electric potential produced by frog heart muscle*, J. Appl. Phys., 57 (1985), pp. 2640–2646.

[8] S. CHUN, *Method of moving frames to solve (an)isotropic diffusion equations on curved surfaces*, J. Sci. Comput., 59 (2013), pp. 626–666.

[9] R. H. CLAYTON, O. BERNUS, E. M. CHERRY, H. DIERCKX, F. H. FENTON, L. MIRABELLA, A. V. PANFILOV, F. B. SACHSE, G. SEEMANN, AND H. ZHANG, *Models of cardiac tissue electrophysiology: Progress, challenges and open questions*, Prog. Biophys. Mol. Biol., 104 (2011), pp. 22–48.

[10] R. W. DOS SANTOS, F. DICKSTEIN, AND D. MARCHESIN, *Transversal versus longitudinal current propagation on a cardiac tissue and its relation to mcg*, Biomed. Tech (Berl), 47 Suppl. Pt 1 (2002), pp. 249–52.

[11] R. W. DOS SANTOS AND H. KOCH, *Interpreting biomagnetic fields of planar wave fronts in cardiac muscle*, Biophys. J., 88 (2005), pp. 3731–3733.

[12] L. P. FERRIS, B. G. KING, P. W. SPENCE, AND H. B. WILLIAMS, *Effect of electric shock on the heart*, Transactions of the American Institute of Electrical Engineers, 55 (1936), pp. 498–515.

[13] R. FITZHUGH, *Impulses and physiological states in theoretical models of nerve membrane*, Biophys. J., 1 (1961), pp. 445–466.

[14] R. FITZHUGH, *Mathematical models of excitation and propagation in nerve. Chapter 1*, McGraw-Hill Book Co., 1969.

[15] J. E. HALL, *Guyton and Hall Textbook of Medical Physiology*, Saunders, 12th revised edition ed., 2010.

[16] J. S. HESTHAVEN AND T. WARBURTON, *Nodal Discontinuous Galerkin Methods*, Springer, 2008.

[17] J. R. HOLZER, L. E. FONG, V. Y. SIDOROV, J. P. W. JR., AND F. BAUDENBACHER, *High resolution magnetic images of planar wave fronts reveal bidomain properties of cardiac tissue*, Biophys. J., 87 (2004), pp. 4326–4332.

[18] J. D. JACKSON, *Classical Electrodynamics*, John Wiley and Sons, third ed., 1998.

[19] J. D. JACKSON, *From lorenz to coulomb and other explicit gauge transformations*, Am. J. Phys., 70 (2002), p. 917.

[20] G. E. KARNIADAKIS AND S. J. SHERWIN, *Spectral/hp element methods for computational fluid dynamics*, Oxford University Press, second ed., 2005.

[21] A. M. KATZ, *Physiology of the heart*, Lippincott Williams and Wilkins, fifth ed., 2010.

[22] J. KEENER AND J. SNEYD, *Mathematical Physiology*, Springer, 1998.

[23] R. M. KIRBY, B. COCKBURN, AND S. J. SHERWIN, *To CG or to HDG: A comparative study*, J. Sci. Compt., 51 (2012), pp. 183–212.

[24] G. T. LINES, M. L. BUIST, P. GROTTUM, A. J. PULLAN, J. SUNDNES, AND A. TVEITO, *Mathematical models and numerical methods for the forward problem in cardiac electrophysiology*, Comput. Vis. Sci., 5 (2003), pp. 215–239.

[25] H. A. LORENTZ, *The theory of electrons and its applications to the phenomena of light and radiant heat*, Leipzig: B. G. Teubner, second ed., 1916.

[26] J. NAGUMO, S. ARIMOTO, AND S. YOSHIZAWA, *An active pulse transmission line simulating nerve axon*, Proc. IRE, 50 (1962), pp. 2061–2070.

[27] R. PLONSEY, *The nature of sources of bioelectric and biomagnetic fields*, Biophys. J., 39 (1982), pp. 309–312.

[28] R. PLONSEY AND R. C. BARR, *Bioelectricity: A quantitative approach*, Springer, third ed., 2007.

[29] E. J. POST, *Formal Structure of Electromagnetics: General Covariance and Electromagnetics*, North-Holland Publishing Company, 1962.

[30] J. M. ROGERS AND A. D. MCCULLOCH, *A collocation-galerkin finite element model of cardiac action potential propagation*, IEEE Trans. Biomed. Eng., 41 (1994), pp. 743– 757.

[31] B. ROTH, *Electrically-silent magnetic fields*, Biophys. J., 50 (1986), pp. 739–745.

[32] B. J. ROTH AND M. C. WOODS, *The magnetic field associated with a plane wave front propagating through cardiac tissue*, IEEE Trans. Biomed. Eng., 46 (1999), pp. 1288–1292.

[33] C. H. RUO AND Y. RUDY, *A model of the ventricular cardiac action potential. depolarization, repolarization, and their interaction*, Circ. Res., 68 (1991), pp. 1501–1526.

[34] G. SCHARF, L. DANG, AND C. SCHARF, *Electrophysiology of living organs from first principles*, arXiv:1006.3453v1, physics.bio-ph (2010).

[35] S. J. SHERWIN, R. M. KIRBY, AND ET. AL., *Nektar++: Open source software library for spectral/hp element method.* Website: http://www.nektar.info.

[36] G. SHOU, L. XIA, M. JIANG, AND J. DOU, *Magnetocardiography simulation based on an electrodynamic heart model*, IEEE Trans. Mag., 47 (2011), pp. 2224–2230.

[37] E. T. WHITTAKER, *A history of the theories of aether and electricity: from the age of Descartes to the close of the Nineteenth century*, Forgotten books, 1910.

[38] J. P. WIKSWO, *Tissue anisotropy, the cardiac bidomain, and the virtual cathode effect*, in Cardiac Electrophysiology, From Cell to Bedside, D. P. Zipes and J. Jalife, eds., W. B., Sanders, Philadelphia, 1995.

[39] R. J. YOUNG, A. V. PANFILOV, AND M. GROMOV, *Anisotropy of wave propagation in the heart can be modeled by a riemannian electrophysiological metric*, PNAS, 107 (2010), pp. 15063–15068.

[40] P. M. ZOLL, A. J. LINENTHAL, W. GIBSON, M. H. PAUL, AND L. R. NORMAN, *Termination of ventricular fibrillation in man by externally applied electric countershock*, N. Engl. J. Med., 254 (1956), pp. 727–732.

[41] P. M. ZOLL, M. H. PAUL, A. J. LINENTHAL, L. R. NORMAN, AND W. GIBSON, *The effects of external electric currents on the heart: control of cardiac rhythm and induction and termination of cardiac arrhythmias*, Circ., 14 (1956), pp. 745–756.

Revised version

This paper is revised to the current form on 1st June, 2016. The original version shows an non-symmetric distribution of the reaction potential ϕ_s due to the wrong boundary implementation for pure Neumann condition. This bug yields slightly different distribution of the electromagnetic field, thus all the figures of electromagnetic field distributions are regenerated with the correct algorithm. However, the main conclusion of the original version is still valid.

ISBN: 978-988-19253-0-5
ISSN: 2078-0958 (Print); ISSN: 2078-0966 (Online)